TriDurLE

National Center for Transportation Infrastructure Durability & Life-Extension

Project ID: 2021-UCD-01

Using Deep Learning for Accurate Detection of Bridge Performance Anomalies

Final Report

by

Yail Jimmy Kim
University of Colorado Denver
1200 Larimer Street, Denver, Colorado, 80217

for

National University Transportation Center TriDurLE
Department of Civil & Environmental Engineering
405 Spokane Street PO Box 642910
Washington State University Pullman, WA 99164-2910

September 24, 2023

Acknowledgements

The research team would like to acknowledge support from the US Department of Transportation through the National Center for Transportation Infrastructure Durability & Life-Extension (TriDurLE). Technical contents presented in this report are based on the opinion of the authors, and do not necessarily represent that of others.

Disclaimer

The contents of this report reflect the views of the authors, who are responsible for the facts and the accuracy of the information presented. This document is disseminated under the sponsorship of the Department of Transportation, University Transportation Centers Program, in the interest of information exchange. The U.S. Government assumes no liability for the contents or use thereof.

Table of Contents

Contents

List of Tables

List of Figures

Executive Summary

This report presents the durability modeling of bridge piers subjected to corrosive environments, including atmospheric, splash, and submerged conditions, for a service period of 100 years. Two types of reinforced concrete columns are utilized, cast-in-place and accelerated bridge construction (ABC), and their time-dependent performance is predicted by von Neumann's square lattice in conjunction with a novel evolutionary mathematics approach called cellular automata. The capacity of the corrosion-damaged columns is upgraded using carbon fiber reinforced polymer (CFRP) sheets. Depending upon concrete strength and construction method, chloride migration mechanisms are evaluated to elucidate the variation of diffusion coefficients, chloride concentrations, and other corrosion-related issues for those columns with and without CFRP-confinement. For the first 30 years, the chloride diffusion of the ABC column is slower than that of the cast-in-place column; otherwise, no difference is noticed. Under the splash condition incorporating periodic wet-dry cycles, chloride concentrations remarkably increase relative to other exposure environments, particularly for the cast-in-place column. The development of corrosion current density is dominated by the pore structure of the concrete, and the corrosion initiation of the ABC column takes 4.3 times longer compared with its cast-in-place counterpart. At 100 years, the capacity of the cast-in-place and ABC columns decreases by 28.1% and 23.2%, respectively, primarily due to the impaired concrete near the degraded reinforcing bars in a corrosion influence zone. The columns' responses are enhanced by CFRP-confinement in terms of toughness, energy dissipation, load-carrying capacity, and load-moment interactions.

Keywords: carbon fiber reinforced polymer (CFRP); cellular automata; column; corrosion; model; rehabilitation; strengthening

1. Introduction

Corrosion is prevalent in built-environments, such as parking garages to highway bridges, and often accompanied by a significant economic impact. It is estimated that more than 3% of the global Gross Domestic Product (GDP), equivalent to $2.5 trillion, is spent due to corrosion[1]. These dollar amounts could include all major aspects of design, construction, and maintenance concerning the corrosion problems of facilities. Corrosion-induced damage often leads to the failure of concrete members, especially when deicing agents are excessively used[2]. When iron-oxide residues surround steel bars, internal pressure causes cracking in the concrete cover[3] through which detrimental chemicals propagate, thereby accelerating the deterioration process, and eventually spalling the cracked concrete[4]. Partially submerged bridge columns are vulnerable to corrosion because wet-dry cycles periodically supply moisture and oxygen[5]. The loss of a column section degrades both strength and ductility[6]; hence, preserving the integrity of structural configurations is an important requirement from a functional standpoint. As far as load-bearing members are concerned, accelerated bridge construction (ABC) is increasingly employed in the infrastructure community, which is a state-of-the-art concept integrating all major aspects of highway bridges. By erecting prefabricated members, transportation agencies benefit from project delivery time, on-site safety, and traffic interruption[7]. The majority of ABC-related research has been focused on seismic responses[8]; accordingly, little is known about other subjects. For example, supported by the fact that the durability of cast-in-place and ABC columns may not be the same on account of different quality control procedures, the need for investigations into corrosion-induced damage in ABC columns was raised recently[9]. Concrete patching and jacketing are traditional repair methods for impaired columns[10], whereas the formation of incipient anodes elevates the likelihood of recurring corrosion problems[11]. In addition, those repairs are labor-intensive and demand considerable preparation for cage fabrication, form assembly, and casting[6,12].

Wrapping with carbon fiber reinforced polymer (CFRP) sheets is an effective approach to upgrade the capacity and ductility of a damaged column by reducing direct exposure to chlorides and minimizing potential corrosion activities in steel reinforcement[13]. When repairing columns possessing disintegrated concrete, surface-preparation should be preceded with a cementitious patching material before applying CFRP in order to warrant even pressure distributions along the substrate[14]. It is necessary to maintain adequate contacts between the concrete and CFRP; otherwise, moisture and chemicals can infiltrate into the locally debonded gap and promote corrosion in the repaired columns. Debaiky et al.[2] tested corrosion rates in reinforced concrete columns with and without CFRP-wrapping. Electrochemical reactions were monitored by the half-cell potential and linear polarization resistance techniques. With one and two layers of CFRP, the corrosion current density of the columns decreased from 10 $\mu A/cm^2$ (65 $\mu A/in.^2$) to 0.1 $\mu A/cm^2$ (0.65 $\mu A/in.^2$). Based on oxygen diffusion and cathodic reactions, Nossoni[3] developed an analytical model to predict the implications of CFRP-wrapping in a corrosive environment. For representing actual site conditions that bring about corrosion, the core of a concrete column was assumed to contain a sufficient amount of chloride before repair. After wrapping with CFRP, a low corrosion rate was noticed in comparison to unconfined specimens and the longevity of the column was extended. Amran et al.[15] reported moisture permeability in CFRP-wrapped concrete, which controlled the degree of corrosion. Pursuant to ASTM C1585[16], permeability coefficients were measured and an empirical expression was proposed. Compared with plain concrete, the presence of CFRP layers significantly lowered the permeability, contingent upon the number of bonded layers. Although CFRP-wrapping was not yet utilized for repairing deteriorated ABC columns, possibly ascribing to their relatively short application history, this rehabilitation method can be applicable to such bridge elements and a precedent assessment would be of interest.

This report discusses the ramifications of corrosion in the simulated performance of cast-in-place and ABC columns under various exposure conditions. Cellular automata, an evolutionary mathematics approach, are adopted to simulate the intricate progression of diffusive chlorides via mutual interactions among multiple discrete entities controlling regional responses, which are instrumental in determining the global behavior of the deteriorated columns. Additionally, the efficacy of CFRP-wrapping is examined with a focus on strength recovery and reductions in chloride ingress rate.

2. Benchmark Column

Pursuant to the American Association of State Highway and Transportation Officials (AASHTO) Load and Resistance Factor Design (LRFD) Bridge Design Specifications (BDS)[19], a simulated two-column bridge pier is designed to support a two-span concrete box girder bridge. Described below are the materials and structural details of the column exposed to aggressive service environments, and a CFRP-strengthening technique for restoring a capacity loss caused by corrosion damage.

2.1. Outline and Parameters

The benchmark column was a circular shape with a diameter of ϕ = 1,070 mm (3.5 ft) at a length of 5.3 m (17.5 ft). Each of No. 14 Grade 60 reinforcements (d_b = 43 mm (1.69 in.), where d_b is the nominal diameter, with a yield strength of f_y = 414 MPa (60 ksi)) had a cross-sectional area of A_s = 1,452 mm^2 (2.25 in.^{2}), and 12 rebars were distributed around the column section (Fig. 1(a)). It was assumed that transverse ties were adequately placed to prevent the local buckling of the longitudinal rebars. In view of practical significance, a variable range of concrete strength was used from f'_c = 30 MPa (4,350 psi) to 45 MPa (6,530 psi). Table 1 enumerates the ingredients of the concrete mixtures based on ACI 211.1-91[20], which were necessary for modeling chloride migration. The cover depth of the column (Table 2) was assigned as specified in AASHTO LRFD BDS[19] along with modification factors in relation to the water-to-cement ratio (*wc*) of the concrete (Table 1). Regarding the construction of the column, cast-in-place and ABC methods were taken into consideration.

2.2. Service Condition

In compliance with NACE SP0176-2007-SG[21], the column was exposed to three service environments: atmospheric, splash, and submerged zones (Fig. 1(b)). The atmospheric zone is not wet, but airborne chlorides permeate the column concrete. The splash zone suffers from the continual fluctuation of water level, accelerating the adverse consequences of wet-dry cycles in tandem with capillary suction and diffusion[22]. The submerged zone is permanently saturated and electrochemical reactions among chlorides, electrolytes, and dissolved oxygen facilitate a corrosion process[23]. The performance of the column under those simulated corrosive environments was examined for 100 years, which can fully cover the design life of 75 years in AASHTO LRFD BDS[19]. It is noteworthy to mention that the 75-year design life was conservatively taken because the actual service life of bridge structures is generally longer than 100 years[24].

2.3. CFRP-Strengthening

The provisions of ACI 440.2R-17[14] were referenced to strengthen the corrosion-damaged column

$$f'_{cc} = f'_c + \psi_f 3.3\kappa_a f_l \quad (1)$$

$$f_l = \frac{2E_f n t_f \varepsilon_{fe}}{\phi} \quad (2)$$

where f'_{cc} is the compressive strength of the confined concrete; ψ_f is the reduction factor (ψ_f = 1 for a nominal capacity prediction); κ_a is the efficiency factor (κ_a = 1 for a circular section); f_l is the confining pressure; E_f, n, and t_f are the elastic modulus, number of plies, and thickness of CFRP, respectively; and ε_{fe} is the effective CFRP strain ($\varepsilon_{fe} = 0.55\varepsilon_{fu}$, in which ε_{fu} is the rupture strain). Commercially available CFRP sheets, consisting of unidirectional carbon fibers and an epoxy resin, were used with the following properties: ultimate strength (f_{fu}) = 3,800 MPa (550 ksi), E_f = 227 GPa (32,900 ksi), ε_{fu} = 0.0167, and t_f = 0.165 mm (0.0065 in.). The damaged column was confined at a capacity loss of 10% and the strengthening effect was maintained up to 100 years (illustrative explanations will be given).

3. Theoretical Modeling

A modeling approach is elaborated on the initiation and progression of corrosion in the benchmark column and corresponding structural responses. The interdependency of axial load and bending moment is delineated for the prediction of the column capacity when linked with unfavorable operational environments.

3.1. Cellular Automata

Cellular automata are a branch of computational mathematics, which are intended to understand the complexity of discrete dynamical systems[25]. The architecture of cellular automata comprises an array of multiple grids in a finite dimension, responding to a preset rule that defines a relationship between adjacent cells. With an increase in time, the assembled cohort evolves with the absence of a governing entity at the global level (that is, the engagement of the constituting cells is completely autonomous) and a generalized pattern is manifested. For the present numerical study, the von Neumann neighborhood with orthogonal cells[26] was chosen to simulate the migration of chlorides in the column concrete. Further information on the development, principle, and application of cellular automata is available elsewhere[27,28].

3.2. Chloride Diffusion

3.2.1. Kinetics

Diffusive interactions among discrete cells may be represented by Fick's second law

$$\frac{\partial C}{\partial t} = D\frac{\partial^2 C}{\partial^2 x^2} \quad (3)$$

where C is the chloride concentration at position x and time t; and D is the diffusion coefficient. Conforming to the von Neumann's square lattice (Fig. 2(a)), the concentration of the center cell at time t+1 ($C_{x,y}(t+1)$) can be estimated by[29]

$$C_{x,y}(t+1) = \Phi_1 C_{x,y}(t) + \Phi_2 C_{x,y-1}(t) + \Phi_3 C_{x+1,y}(t) + \Phi_4 C_{x,y+1}(t) + \Phi_5 C_{x-1,y}(t) \quad (4)$$

$$\sum_{i=1}^{5} \Phi_i = 1 \quad (5)$$

where x and y are the abscissa and ordinate of the two-dimensional space, respectively, and Φ_i is the evolutionary coefficient satisfying the principle of mass conservation (Eq. 5). Assuming that the progression of chlorides is isotropic[30], $\Phi_1 = 0.5$ for $C_{x,y}$ and $\Phi_{2,3,4,5} = 0.125$ are suggested with Eq. 6[29]

$$\Delta t = \Phi_i \frac{\Delta s}{D} \tag{6}$$

where Δt is the time step and Δs is the size of the cell. The outbound coefficient Φ_6 from the center cell ($C_{x,y}$) is obtained by $\Phi_6 = (1 - \Phi_1)/4$. The initial and time-dependent diffusion coefficients ($D(0)$ and $D(t)$, respectively) of ordinary concrete may be determined by[31,32]

$$D(0) = ke^{\left(-\sqrt{10/wc}\right)} \tag{7}$$

$$D(t) = D_e(0)t^{-\eta} \tag{8}$$

$$\eta = k_a(1 - 1.5wc) \tag{9}$$

where k and k_a are the service environment and adjustment factors, respectively (k = 10,000 mm^2/year (15.5 in.^{2}/year) and k_a = 1.0 for atmosphere, k = 15,000 mm^2/year (23.3 in.^{2}/year) and k_a = 0.1 for splash, and k = 25,000 mm^2/year (38.8 in.^{2}/year) and k_a = 0.6 for submerged conditions); and $D_e(t)$ is the diffusion coefficient under a specific exposure environment; and η is the age coefficient. Considering the different curing conditions of concrete between the cast-in-place and ABC columns, Eq. 10 is adopted

$$D_e(0) = k_c D(0) \tag{10}$$

where k_c is the curing factor (k_c = 1 for the concrete that is moisture-cured for 28 days, representing ABC members, and k_c = 4.3, 2.8, and 2.7 for the cast-in-place concrete (cured under a typical site condition at a relative humidity of 40% to 50% and 19ºC (66ºF) to 23ºC (73ºF)) that is subsequently exposed to atmospheric, splash, and submerged conditions, respectively[33].

3.2.2. Validation

The above-described approach was validated against other research programs[35-38]. According to the properties listed in Table 3, chloride contents were computed at the respective chloride-exposure times and locations denoted in the cited literature (Fig. 3). It should be noted that, for the purpose of consistency, the units of the contents were intentionally kept as presented in the literature. In spite of the marginal differences possibly due to randomly dispersed aggregates in the concrete specimens, the prediction was sufficiently close to the collated data.

3.3. Corrosion

3.3.1. Initiation

The corrosion initiation of the column may be attained by[39,40]

$$t_i = \frac{(c/10)^2}{4D}\left(erf^{-1}\left(\frac{C_{cr} - C_0}{C_i - C_0}\right)\right)^{-2} \text{ for atmospheric and submerged conditions} \tag{11a}$$

$$t_i = \left(\frac{\ln(1.08 i_{corr}) - 8.37 - 0.618 \ln 1.69 C_f(t) + 3034/T + 0.000105 R_c}{2.32} \right)^{0.215} \quad \text{for splash} \qquad (11b)$$

where t_i is the initiation time; c is the concrete cover in mm; *erf* is the Gauss error function; C_{cr} and C_i are the critical and initial chloride concentrations, respectively (C_{cr} = 0.4% and C_i = 0% of the cement weight[41]); C_0 is the surface chloride concentration; i_{corr} is the corrosion current density (i_{corr} = 0.3 $\mu A/cm^2$ (1.94 $\mu A/in.^2$) was adopted[42]); C_f is the free chloride concentration at the rebar level in kg/m^3; T is the absolute temperature at the surface of the rebar in Kelvin (T = 293.15K); and R_c is the resistance of the cover concrete in ohms (R_c = 1,500 ohms). For the atmospheric and submerged conditions, the surface chlorides were assumed to be constant (C_0 = 0.2% and 0.5% of the concrete weight, respectively[43]); however, for the splash exposure, variable chlorides were considered to reflect periodic wet-dry cycles with time t in years alongside the percent weight of the concrete[44,45]

$$C_0(t) = (0.213wc + 0.134)t^{0.484} \qquad (12)$$

3.3.2. Progression

Upon initiation of corrosion damage, the cross-sectional area of the reinforcement is reduced[46]

$$d_b(t) = d_{bo} - 0.0232(t - t_i) i_{corr} \qquad (13)$$

where $d_b(t)$ and d_{b0} are the diameter of the rebar at time t and its initial counterpart, respectively. The corrosion current density (i_{corr}) with increasing corrosion time t in years may be calculated using Eq. 14 that was originated from 2,927 measured data at the surface of steel rebars for up to 5 years of outdoor exposure[40]

$$\ln(1.08 i_{corr}) = 8.37 + 0.618 \ln 1.69 C_f(t) - 3034/T - 0.000105 R_c + 2.32 t^{-0.215} \qquad (14)$$

Although Eq. 14 is comprehensive, several limitations are acknowledged because it did not account for geometry, oxygen availability, the dynamic nature of corrosion, and other factors that influence corrosion rate. Since the free chlorides (C_f) affect the progression of corrosion, the total chlorides imparted from the cellular automata model (C_t) in kg/m^3 need to be converted[47]

$$C_f = 0.8541 C_t \qquad (15)$$

When the column is wrapped with CFRP, the ingress of chlorides is impeded and previous research demonstrates that the magnitude of the current density decreases by 1/3[48].

3.3.3. Impaired Concrete

The volumetric expansion of the corroded rebars weakens the cover concrete of the column. For modeling convenience, the occurrence of cracking and spalling is frequently replaced by the equivalent compressive strength ($f_c^*(t)$) of the cover concrete[49,50]

$$f_c^*(t) = \frac{f_c'}{1 + k^* \varepsilon_1(t)/\varepsilon_{co}} \qquad (16)$$

where k^* is the characteristic coefficient ($k^* = 0.1$); ε_{co} is the strain at the peak stress of the concrete ($\varepsilon_{co} = 0.002$); and $\varepsilon_1(t)$ is the average tensile strain of the cracked concrete[50]

$$\varepsilon_1(t) = (n_b W_{cr}(t))/\phi \tag{17}$$

where n_b is the number of the rebars in compression and $W_{cr}(t)$ is the average crack width in mm[51]

$$W_{cr}(t) = K\left(\Delta A_s(t) - \Delta A_{so}\right) \tag{18}$$

where K is an empirical factor ($K = 0.00575$/mm); $\Delta A_s(t)$ is the cross-sectional loss of the rebars in mm^2; and ΔA_{so} is the loss of the rebar section in mm^2 when the column concrete cracks

$$\Delta A_{so} = A_{so}\left(1 - \left(1 - \frac{\alpha_p}{d_{bo}} x_0 10^{-3}\right)^2\right) \tag{19}$$

where A_{so} is the cross-sectional area of the intact steel rebars; α_p is the pitting factor ($\alpha_p = 2$ for uniform corrosion); and x_0 is the corrosion penetration in μm associated with cover depth c in mm[52]

$$x_0 = 7.53 + 9.32(c/d_{bo}) \tag{20}$$

The pitting type of corrosion in Eq. 19 is attributed to the interaction between the chloride ions (Cl^-) and iron hydroxide ($Fe(OH)_2$), which generates autocatalytic reactions[53].

3.4. Structural Model

3.4.1. Load-Bearing

The nominal capacity of the column ($P_n(t)$) under axial compression is calculated

$$P_n(t) = 0.85\left[A_s(t) f_y + 0.85\left(f_c'\left(A_g - A_s(t) - A_{iz}\right) + f_c^*(t) A_{iz}\right)\right] \tag{21}$$

$$A_{iz} = n_b\left(\frac{\left(360^o - 2\left(90^0 - \theta^o\right)\right)}{360^o}\pi c_r^2 - 2A_r\right) \tag{22}$$

$$A_r = \frac{\pi\left(\phi/2 - c_r\right)^2 \theta^o}{360^o} - \frac{c_r^2/\tan\theta^o}{2} \tag{23}$$

$$\sin\theta^o = \frac{c_r}{\phi/2 - c_r} \tag{24}$$

where A_g is the gross cross-sectional area of the column; A_{iz} is the area of the influence zone for $f_c^*(t)$ in Eq. 16 (Figs. 4(a) and (b)); n_b is the number of the rebars; c_r is the distance from the concrete surface to the rebar center; A_r is the difference between the arc and triangular areas (Fig. 4(c)); and θ is the angle of the component triangle in degrees. As noted earlier, the equivalent strength of $f_c^*(t)$ in the influence zone

(A_{iz}) is activated when the concrete cracks, and the reduced strength reflects the accelerated chloride ingress in the cracked column.

The axial capacity of the column is independently computed by the cellular automata model (Eq. 25) and verified against Eq. 21

$$P_n(t) = \left(\sum_{j=1}^{j=n_c}\sum_{i=1}^{i=n_c}\sigma_{c,i,j}(t) + \sum_{j=1}^{j=n_s}\sum_{i=1}^{i=n_s}\sigma_{s,i,j}(t)\right)A_a \quad (25)$$

where i and j are the abscissa and ordinate, respectively, in Fig. 5(a); n_c and n_s are the number of agents for the concrete and steel reinforcement, respectively; A_a is the area of a single agent; and $\sigma_{c,i,j}(t)$ and $\sigma_{s,i,j}(t)$ are the stress in the concrete and steel, respectively

$$\sigma_{c,i,j}(t) = f'_{c,i,j}\left[\frac{2\varepsilon_{c,i,j}(t)}{\varepsilon_{co}} - \left(\frac{\varepsilon_{c,i,j}(t)}{\varepsilon_{co}}\right)^2\right] \quad (26)$$

$$\sigma_{s,i,j}(t) = \varepsilon_{s,i,j}(t)E_s \le \sigma_y \quad (27)$$

where $f'_{c,i,j}$ is the compressive strength of the concrete agent $a_{c,i,j}$ at time t (f'_c and $f_c^*(t)$ are used for the core and the impaired area, respectively, Fig. 4); E_s and σ_y are the elastic modulus and yield strength of the steel (E_s = 200 GPa (29,000 ksi) and σ_y = 414 MPa (60 ksi)); $\varepsilon_{c,i,j}(t)$ is the strain of $a_{c,i,j}$; and $\varepsilon_{s,i,j}(t)$ is the strain of the steel agent $a_{s,i,j}$ (Figs. 5(a) to (c)). The moment capacity of the column ($M_n(t)$) is expressed in a similar manner

$$M_n(t) = \left(\sum_{j=1}^{j=n_c}\sum_{i=1}^{i=n_c}\sigma_{c,i,j}(t) + \sum_{j=1}^{j=n_s}\sum_{i=1}^{i=n_s}\sigma_{s,i,j}(t)\right)A_a\left(\frac{\phi}{2} - j_a\right) \quad (28)$$

where j_a is the ordinate of the agent.

3.4.2. Interaction Diagram

The capacity of the column can be obtained under compression (P_n) and flexural (M_n) loadings. The pure compression of the section is associated with the uniform strain of ε_{cu} = 0.003, in which ε_{cu} is the maximum usable strain of concrete[54]. For other general cases, the steel strain at the bottom of the section (ε_s in Fig. 5(c)) is incremented and, then, the aforementioned $\varepsilon_{i,j}$ strain is determined

$$\varepsilon_{i,j} = \frac{(\varepsilon_s + \varepsilon_{cu})\left(\frac{\varepsilon_{cu}}{\varepsilon_{cu} + \varepsilon_s} d_{br} j_a\right)}{d_{br}} \quad (29)$$

where d_{br} is the distance from the top of the section to the bottom rebar (Fig. 5(c)). For the CFRP-confined column, the interaction diagram may be constructed in accordance with the procedure explained in ACI 440.2R-17[14]. To accommodate the equivalent compressive strength (Eq. 16) within the influence zone (A_{iz}), the unconfined concrete strength (f'_c) in Eq. 1 is replaced by

$$f_i'(t) = \left(f_c'\left(A_g - A_s(t) - A_{iz}\right) + f_c^*(t)A_{iz} \right) / A_g \quad (30)$$

where f_i' is the adjusted concrete strength for CFRP-confinement with corrosion damage.

4. Implementation

The durability of cast-in-place and ABC columns, predicted by discrete computational cellular automata models, is expounded from material and structural points of view. Emphasis is placed on the diffusivity of chlorides, consequences of corrosion, and the efficaciousness of CFRP-strengthening.

4.1. Chloride Migration

4.1.1. Diffusion

The coefficients of chloride diffusion are provided in Figs. 6(a) and (b) for the cast-in-place and ABC columns, respectively. The exponentially diminishing coefficients illustrate that the concrete pores became partially clogged by surplus chlorides over time; in other words, the permeated chlorides reduced the effective porosity of the cement binder[55]. As the compressive strength of the concrete was increased from 30 MPa (4,350 psi) to 45 MPa (6,530 psi), the flux of the chlorides noticeably dropped (Fig. 6(a)). This observation aligns with the fact that greater hydration in concrete leads to a strength gain and decreases the size of micro-pores; consequently, the transport of chloride ions in the electrolytes is retarded[56,57]. Compared with the cast-in-place column, the diffusion coefficient of the ABC column was lower (Fig. 6(b)) and the submerged condition showed a consistently higher coefficient than other environments, owing to the increased conductivity of the pore solution[58]. Likewise, the rate of the diffusion coefficient rapidly developed under the submerged condition for the cast-in-place column (Fig. 6(c)); whereas, marginal differences were noted among the three environments after 30 years (Fig. 6(c), inset). Shown in Fig. 6(d) is a comparison between the diffusion coefficient rates of the cast-in-place and ABC columns. Irrespective of concrete strength (f'_c = 30 MPa (4,350 psi) and 45 MPa (6,530 psi)), the ABC column outperformed and its peak rates were 37% of those of the cast-in-place column, on average.

4.1.2. Concentration

The chloride concentrations of the cast-in-place column at the level of steel surface are plotted in Figs. 7(a) and (b), dependent upon concrete strength and exposure condition, respectively. The ingress of chlorides in the column with f'_c = 30 MPa (4,350 psi) was 1.9 times relative to the case with f'_c = 45 MPa (6,530 psi) at 100 years (Fig. 7(a)). The high water-to-cement ratio of the low strength concrete (Table 1) allowed more chlorides on account of the increased permeability[59]. In regard to the environmental exposure (Fig. 7(b)), the concentration was prominent under the splash condition because the wet-dry cycles expedited the sorptivity of the concrete[60]. As concrete resistance to chlorides declines when saturated[61], the asymptotic concentration curve under the submerged condition was graphed above the curve under the atmospheric condition. It is worth noting that, even if both were subjected to water, the mechanisms of chloride progression under the splash and submerged conditions differed: the former was based on absorption and capillary suction, while the latter was related to pure diffusion caused by a concentration gradient in the electrolyte across the column[62].

Figure 7(c) exhibits the elevation of chloride concentrations in the cast-in-place and ABC columns under the submerged condition. The response slope of the cast-in-place column was steep up to 12 years, followed by a transition to the gradually rising concentrations. Except for the distinguishable development trend between 0 and 30 years, the slopes of these column categories were virtually identical, meaning that

the superior durability of the ABC column was due to the betterment of its performance during the relatively early ages. For this reason, the ABC column allowed less chlorides inside the concrete (Fig. 7(d)). A comprehensive summary of the chloride concentrations at a depth of 100 mm (4 in.), the average cover of the columns, is charted in Figs. 7(e) and (f). The use of ABC was beneficial for all occasions, especially under the splash condition.

4.2. Effects of Corrosion

4.2.1. Corrosion Current Density

The ascending pattern of the corrosion current density was a function of the concrete strength (Fig. 8(a)), which is concerned with the connectivity of the micro-pores that dominates the transport of chloride ions[55]. The difference in the initial diffusion coefficient ($D(0)$ in Table 2) was responsible for the grouping of the densities above and below the concrete strength of f'_c = 40 MPa (5,800 psi). Figure 8(b) reaffirms that the alternate cycles of saturation and desiccation raised the conductivity of the micro-pores with the dissolved chloride ions[63], thereby lessening the resistivity of the column concrete under the splash condition (that is, the increased corrosion rate). Such a prediction, however, does not necessarily signify invariant local conductivity since the activation energy of the concrete oscillated as per the degree of saturation[30]. The evolution tendency of the current density under the submerged condition in Fig. 8(b) clarifies the importance of continued oxidation for the electrochemical process of corrosion: the plateau-like response was attributable to the limited supply of oxygen in the pores that partially filled with chlorides, which slowed down cathodic reactions[64]. Shown in Fig. 8(c) are the corrosion current densities normalized by time. The growth rate of the density for the cast-in-place column was rapider than the rate for the ABC column, whereas their dissimilarity disappeared after 40 years. It is thus stated that the high current density of the cast-in-place column (Fig. 8(d)) was the result of the accelerated rate before the 40-year alteration time.

4.2.2. Detrimental Consequences

Figure 9(a) demonstrates the corrosion initiation year of the cast-in-place column. Under the splash and submerged conditions that were linked with direct contact to water, the initiation time was 11 years, on average. Contrarily, the initiation time under the atmospheric condition was longer than 54 years and the case with a concrete strength higher than 40 MPa (5,800 psi) would not corrode within the 75-year design life of AASHTO LRFD BDS[19]. The corrosion initiation of the ABC column took substantially longer, up to 4.3 times that of the cast-in-place column (Fig. 9(b)). Once the columns corroded, the diameter of the reinforcing bars began to dwindle (Fig. 9(c)) and the use of the ABC technique remarkably inhibited a reduction magnitude (Fig. 9(d)). The strength decrease of the equivalent cover concrete for the cast-in-place column was noticed at 16.5 years and 15.4 years under the splash and submerged conditions, respectively (Fig. 9(e)), which were incomparable with the case under the atmospheric exposure (> 62 years). As shown in Fig. 9(f), the ratio of the cover-strength reduction time between the ABC and cast-in-place columns was over 1.56 (no reduction occurred for the ABC column with a concrete strength greater than 35 MPa (5,080 psi)).

4.3. Structural Aspect

4.3.1. Axial Capacity

The reduced capacity of the cast-in-place column under the splash condition inducing corrosion is provided in Fig. 10(a). The ratio of the capacities between the damaged and undamaged states diminished with time. It should be noted that the proximity of the responses with f'_c = 35 MPa (5,080 psi) and 40 MPa (5,800 psi) resulted from the same cover depth of 100 mm (4 in.), Table 2. The contribution of each

constituent to the capacity drop is visible in Figs. 10(b) and (c). The capacity variation caused by the equivalent compressive strength (Eq. 16) was the primary factor (Fig. 10(b)), while the influence of the steel corrosion was marginal (Fig. 10(c)). In particular, the dependency of the concrete strength pertaining to the chloride flux was significant on the capacity decrease of the column exposed to water (the splash and submerged conditions, Fig. 10(d)). The benefit of the ABC column was pronounced for a low strength concrete; for instance, the capacity-drop ratios between the ABC and cast-in-place columns under the submerged condition were 0.88 and 0.67 for f'_c = 30 MPa (4,350 psi) and 45 MPa (6,530 psi), respectively (Fig. 10(e)).

4.3.2. Effectiveness of CFRP-Confinement

Complying with the provisions of ACI 440.2R-17[14] (Eqs. 1 and 2), the number of CFRP layers was calculated and then rounded for practical application (Fig. 11(a)). The more durable ABC column necessitated less layers than the cast-in-place column, and the propensity was preserved without regard to the strength of the unconfined concrete (f'_c). The constitutive relationship of the confined concrete (Fig. 11(b)) was bilinear until the maximum useable strains of CFRP were reached (all values did not exceed the strain limit of 0.01 specified in ACI 440.2R-17[14]). Although the increased f'_c from 30 MPa (4,350 psi) to 45 MPa (6,530 psi) raised the confined strength (f'_{cc}), the usable strain was shortened from ε_{ccu} = 0.0065 to 0.0044. An average toughness ratio of 1.97 was noted between the confined and unconfined cases (toughness is defined as the area under a stress-strain curve up to failure); scilicet, CFRP-confinement improved the energy dissipation of the column concrete. Figures 11(c) and (d) show the time-dependent capacity ratio of the cast-in-place and ABC columns, respectively. In line with the strengthening philosophy established earlier, the columns were strengthened when a 10% reduction was noticed in the capacity and the enhanced ratios were maintained above unity for the rest of service life to 100 years (confined capacity ≥ intact capacity). The temporal span of the adjusted capacity ratio for the cast-in-place column (27.4 years to 100 years) was 46.4% longer than the span for the ABC column (50.4 years to 100 years); on the contrary, the efficacy of strengthening was indistinguishable, which corroborates the fact that CFRP-based rehabilitation is a recommendable technique for both column types.

4.3.3. Load-Moment Interaction

The interaction diagram of the axial load (P_n) and bending moment (M_n) for the cast-in-place column at 100 years is given in Fig. 12(a). The size of the interaction envelope conspicuously decreased under the splash condition. With CFRP-confinement, the envelope was enlarged over the control curve, indicating the fully recovered performance of the abated column. The abruptly dropping moment at the balance point of the confined column (P_b and M_b) was ascribed to the restriction of ACI 440.2R-17[14]: strength enhancement is only allowed in the compression-controlled region. As the core strength (f'_c) was increased (Fig. 12(b)), the resistance level of the upgraded column became elevated against the combined axial compression and bending. The ABC column exhibited structural efficiency with less CFRP layers (Fig. 12(c)). The transition moment from compression- to tension-controlled failure modes went up in proportion to the core strength (Fig. 12(d)) and, albeit inappreciable, the ABC column outperformed the cast-in-place column.

5. Summary and Conclusions

This report has investigated the detrimental effects of chloride migration in cast-in-place and ABC column models exposed to atmospheric, splash, and submerged environments. Employing a novel simulation approach called cellular automata, chloride diffusivity and various levels of corrosion were computed during a service period of 100 years. The degraded columns were strengthened with CFRP sheets in

conformity with ACI 440.2R-17[14] and their load-carrying capacity was examined. Attention was directed toward full-range interactions between axial and flexural loadings. The study substantiated that CFRP-confinement was a favorable technique for both column types. The following are concluded:

- Because of the concrete pores partially filled by surplus chlorides as documented in the literature, the diffusion coefficient of the columns exponentially decreased with time. The microstructural characteristics of the concrete relating to the compressive strength also dominated the ingress of chlorides. The chloride diffusion of the ABC column was slower than that of the cast-in-place column; however, their distinction in the diffusion rate disappeared after 30 years.
- The chloride concentration of the columns under the splash condition was noticeable owing to the expedited sorptivity of the concrete subjected to wet-dry cycles, which was properly documented by others. The development of chloride concentrations in the cast-in-place column was faster than the case of the ABC column, which led to the superior durability of the latter particularly under the splash exposure.
- The corrosion current density of the columns steadily rose up to 100 years, while the growth pattern was a function of the concrete strength related to the connectivity of micro-pores. Compared with the ABC column, the cast-in-place column revealed a rapid increase rate in the current density until 40 years, beyond which both cases showed similar responses.
- When the cast-in-place column was exposed to water (splash and submerged), the average corrosion initiation time was 11 years. By contrast, the ABC column required up to a 4.3 times longer period and effectively impeded a loss in the cross-sectional area of the reinforcement. The reduction of the equivalent strength due to corrosion-induced cracking and spalling was not noticed for the ABC column with a concrete strength of 35 MPa (5,080 psi) and greater.
- With the presence of corrosion damage, the axial capacity of the cast-in-place and ABC columns decreased by 28% and 23% under the splash condition at 100 years, respectively. The primary factor for such an observation was the impaired concrete in the corrosion influence zone, whereas the direct contribution of the deteriorated reinforcement was less than 5%.
- The CFRP-strengthening raised the toughness of the existing concrete by almost two times; accordingly, the confined columns were able to carry more moments without flexural failure. Notwithstanding the reduced number of CFRP layers, the ABC column's performance was comparable to that of the cast-in-place column under synergistic distress from axial compression and bending.

References

[1] Koch, G., Varney, J., Thompson, N., Moghissi, O., Gould, M., and Payer, J. 2016. International measures of prevention, application and economics of corrosion technology, NACE International, Houston, TX.

[2] Debaiky, A.S., Green, M.F., and Hope, B.B. 2002. Carbon fiber-reinforced polymer wraps for corrosion control and rehabilitation of reinforced concrete columns, ACI Materials Journal, 99(2), 129-137.

[3] Nossoni, G. 2015. Modeling the corrosion rate of steel reinforcement in FRP-wrapped concrete, Journal of Composites for Construction, 20(3), 04015068.

[4] Chen, E., Tang, S., and Leung, C.K.Y. 2019. Corrosion-induced cracking in reinforced concrete due to chloride contamination and ingress, ACI Materials Journal, 116(5), 99-111.

[5] Hussain, R.R., Al-Negheimish, A., Alhozaimy, A., and Singh, D.D.N. 2020. Corrosion characteristics of vanadium micro-alloyed steel reinforcement bars exposed in concrete environments and industrially polluted atmosphere, Cement and Concrete Composites, 113, 103728.

[6] Hamilton, C.H., Pardoen, G.C., Navalpakkam, S., and Kanzanjy, R.P. 2004. Reinforced concrete bridge column performance enhancement through shotcrete jacketing, ACI Structural Journal, 101(3), 332-340.

[7] Khan, M.A. 2014. Accelerated bridge construction: best practices and techniques, Butterworth-Heinemann, Oxford, UK.

[8] Zhang, Q. and Alam, M.S. 2020. State-of-the-art review of seismic-resistant precast bridge columns, Journal of Bridge Engineering, 25(10), 03120001.

[9] Liu, R. and Palermo, A. 2020. Ten years of experiments on bridges using resilient damage-resistant systems and accelerated construction techniques, Structural Engineering International, 30(2), 224-231.

[10] Grantham, M., Mechtcherine, V., and Schneck, U. 2012. Concrete solutions, CRC Press, London, UK.

[11] Christodoulou, C., Goodier, C., Austin, S., Webb, J., and Glass, G.K. 2013. Diagnosing the cause of incipient anodes in repaired reinforced concrete structures, Corrosion Science, 69, 123-129.

[12] Bousias, S.N., Biskinis, D., Fardis, M.N., and Spathis, A.-L. 2007. Strength, stiffness, and cyclic deformation capacity of concrete jacketed members, ACI Structural Journal, 104(5), 521-531.

[13] ElMaaddawy, T., Chahrour, A., and Soudki, K. 2006. Effect of fiber-reinforced polymer wraps on corrosion activity and concrete cracking in chloride-contaminated concrete cylinders, Journal of Composites for Construction, 10(2), 139-147.

[14] ACI. 2017. Guide for the design and construction of externally bonded FRP systems for strengthening concrete structures (ACI 440.2R-17), American Concrete Institute, Farmington Hills, MI.

[15] Amran, Y.H.M., Alyousef, R., Alabduljabbar, H., Alaskar, A., and Alrshoudi, F. 2020. Properties and water penetration of structural concrete wrapped with CFRP, Results in Engineering, 5, 100094.

[16] ASTM. 2004. Standard test method for measurement of rate of absorption of water by hydraulic-cement concretes (ASTM C1585-04), ASTM International, West Conshohocken, PA.

[17] Ramirez, J.L. 1996. Ten concrete column repair methods, Construction and Building Materials, 10(3), 1996.

[18] Karimipour, A. and Edalati, M. 2021. Retrofitting of the corroded reinforced concrete columns with

CFRP and GFRP fabrics under different corrosion levels, Engineering Structures, 228, 111523.

[19] AASHTO. 2020. AASHTO LRFD bridge design specifications (9th edition), American Association of State Highway Transportation Officials, Washington, D.C

[20] ACI. 2009. Standard practice for selecting proportions for normal, heavyweight, and mass concrete (ACI 211.1-91: reapproved 2009), American Concrete Institute, Farmington Hills, MI.

[21] NACE. 2007. Corrosion control of submerged areas of permanently installed steel offshore structures associated with petroleum production (SP0176-2007-SG), National Association of Corrosion Engineers, Houston, TX.

[22] Gao, J., Yu, Z., Song, L., Wang, T., and Wei, S. 2013. Durability of concrete exposed to sulfate attack under flexural loading and drying-wetting cycles, Construction and Building Materials, 39, 33-38.

[23] Eyu, G.D., Will, G., Dekkers, W., and MacLeod, J. 2017. Effect of dissolved oxygen and immersion time on the corrosion behaviour of mild steel in bicarbonate/chloride solution, Materials, 9(9), 748.

[24] Freyermuth, C. 2009. Service life and sustainability of concrete bridges, ASPIRE, 3(4), 12-15.

[25] Wolfram, S. 1984. Cellular automata as models of complexity, Nature, 311(5985), 419-424.

[26] Wolnik, B. and Baets, B.D. 2020. Ternary reversible number-conserving cellular automata are trivial, Information Sciences, 513, 180-189.

[27] Hoekstra, A.G., Kroc, J., and Sloot, P.M.A. 2010. Simulating complex systems by cellular automata, Springer, Heidelberg, Germany.

[28] Baetens, J.M. and Kutrib, M. 2018. Cellular automata and discrete complex systems, Springer, Cham, Switzerland

[29] Podrouzek, J. and Teply, B. 2008. Modelling of chloride transport in concrete by cellular automata, Engineering Mechanics, 15(3), 213-222.

[30] Wang, Y., Gong, F., Zhang, D., and Ueda, T. 2016. Estimation of ice content in mortar based on electrical measurements under freeze-thaw cycle, Journal of Advanced Concrete Technology, 14, 35-46.

[31] Frederiksen, J.M., Mejlbro, L., and Poulsen, E. 2000. The HETEK model of chloride ingress into concrete made simpler by approximations, International RILEM Workshop on Testing and Modelling the Chloride Ingress into Concrete, 317-336.

[32] Poulsen, E. and Mejlbro, L. 2006. Diffusion of chloride in concrete: theory and application. Taylor and Francis, New York, NY.

[33] Alizadeh, R., Ghods, P., Chini, M., Hoseini, M., Ghalibafian, M., and Shekarchi, M. 2008. Effect of curing conditions on the service life design of RC structures in the Persian Gulf region, Journal of

Materials in Civil Engineering, 20(1), 2-8.

[34] Wu, L., Wang, Y., Wang, Y., Ju, X., and Li, Q. 2020. Modelling of two-dimensional chloride diffusion concentrations considering the heterogeneity of concrete materials, Construction and Building Materials, 243, 118213.

[35] Cao, J., Wang, Y., Li, K., and Ma, Y. 2012. Modeling the diffusion of chloride ion in concrete using cellular automaton, Journal of Materials in Civil Engineering, 24 (6), 783-788.

[36] Titi, A., and Biondini, F. 2016. On the accuracy of diffusion models for life-cycle assessment of concrete structures, Structure and Infrastructure Engineering, 12(9), 1202-1215.

[37] Wang, Y., An, M., Yu, Z., Han, B., and Ji, W. 2018. Experimental and cellular-automata-based analysis of chloride ion diffusion in reactive powder concrete subjected to freeze-thaw cycling, Construction and Building Materials, 172, 760-769.

[38] Yin, G., and Pan., L. 2020. The effect of shape on chloride penetration of circular reinforcement concrete columns and its durability design, Applied Sciences 10(2): 459.

[39] Thoft-Christensen, P., Jensen, F.M., Middleton, C.R., and Blackmore, A. 1996. Assessment of the reliability of concrete slab bridges, 7th IFIP WG 7.5 Working Conference, Boulder, CO, 1-8.

[40] Liu, T. and Weyers, R.W. 1998. Modeling the dynamic corrosion process in chloride contaminated concrete structures, Cement and Concrete Research, 28(3), 365-379.

[41] Elsener, B. and Angst, U. 2016. Corrosion inhibitors for reinforced concrete, Science and Technology of Concrete Admixtures, 321-339.

[42] Yoon, S., Wang, K., Weiss, W.J., and Shah, S.P. 2000. Interaction between loading, corrosion, and serviceability of reinforced concrete, ACI Materials Journal, 97(6), 637-644.

[43] Roy, S.K., Chye, L.K., and Northwood, D.O. 1993. Chloride ingress in concrete as measured by field exposure tests in the atmospheric, tidal and submerged zones of a tropical marine environment, Cement and Concrete Research, 23(6), 1289-1306.

[44] Song, H.W., Chang, H.L., and Ann, K.Y. 2008. Factors influencing chloride transport in concrete structures exposed to marine environments, Cement and Concrete Composites, 30(2): 113-121.

[45] Liu, Q., Hu, Z., Lu, X., Yang, J., Azim, I., and Sun, W. 2020. Prediction of chloride distribution for offshore concrete based on statistical analysis, Materials, 13(1), 174, 16 pp.

[46] Val, D.M. and Melchers, R.E. 1997. Reliability of deteriorating RC slab bridges, Journal of Structural Engineering, 123(12), 1638-1644.

[47] Cheewaket, T., Jaturapitakkul, C and Chalee, W. 2010. Long term performance of chloride binding capacity in fly ash concrete in a marine environment, Construction and Building Materials, 24(8), 1352-

1357.

[48] Suh, K., Mullins, G., Sen, R., and Winters, D. 2007. Effectiveness of fiber-reinforced polymer in reducing corrosion in marine environment, ACI Structural Journal, 104 (1), 76-83.

[49] Vecchio, F.J., and Collins, M.P. 1986. Modified compression-field theory for reinforced concrete elements subjected to shear, Journal of the American Concrete Institute, 83(2), 219-231.

[50] Coronelli, D., and Gambarova, P. 2004. Structural assessment of corroded reinforced concrete beams: modeling guidelines, Journal of Structural Engineering, 130(8),1214-1224.

[51] Vidal, T., Castel, A., and François, R., 2004. Analyzing crack width to predict corrosion in reinforced concrete, Cement and Concrete Research, 34(1), 165-174.

[52] Alonso, C., Andrade, C., Rodriguez, J and Diez, J.M. 1998. Factors controlling cracking of concrete affected by reinforcement corrosion, Material and Structures, 31, 435-441

[53] Ahmad, A. and Kumar, A. 2013. Chloride ion migration/diffusion through concrete and test methods, International Journal of Advanced Scientific and Technical Research, 3(6), 151-180.

[54] ACI. 2019. Building code requirements for structural concrete and commentary (ACI 318-19), American Concrete Institute, Farmington Hills, MI.

[55] Koleva, D.A., Copuroglu, O., van Breugel, K., Ye, G., de Wit, J.H.W. 2008. Electrical resistivity and microstructural properties of concrete materials in conditions of current flow, Cement and Concrete Composites, 30, 731-744.

[56] Purnell, P. 2007. Degradation of fibre-reinforced cement composites, Durability of Concrete and Cement Composites, Elsevier, 316-363.

[57] Shi, Y., Chen, X., Li, J., Li, X., and Peng, Z. 2019. Micro–macro properties of plastic concrete anti-seepage wall materials mixed with low-liquid limit clay, Advances in Mechanical Engineering, 11(5), 1-9.

[58] Zhang, Y., Zhang, M., and Ye, G. 2018. Influence of moisture condition on chloride diffusion in partially saturated ordinary Portland cement mortar, Materials and Structures, 51:36.

[59] Espinoza-Hijazin, G. and Lopez, M. 2011. Extending internal curing to concrete mixtures with W/C higher than 0.42, Construction and Building Materials, 25, 1236-1242.

[60] Stanish, K.D., Hoonton, R.D., and Thomas, M.D.A. 1997. Testing the chloride penetration resistance of concrete: a literature review, Report No. DTFH61-97-R-00022, Federal Highway Administration, Washington, D.C.

[61] Basheer, P.A.M., Gilleece, P.R.V., Long, A.E., and McCarter, W.J. 2002. Monitoring electrical resistance of concretes containing alternative cementitious materials to assess their resistance to chloride

penetration, Cement and Concrete Composites, 24, 437-449.

[62] Andrade, C. 1993. Calculation of chloride diffusion coefficients in concrete from ionic migration measurements, Cement and Concrete Research, 23, 724-742.

[63] Cosoli, G., Mobili, A., Tittarelli, F., Revel, G.M., and Chiariotti, P. 2020. Electrical resistivity and electrical impedance measurement in mortar and concrete elements: a systematic review, Applied Sciences, 10, 9152.

[64] Hornbostel, K., Larsen, C.K., and Geiker, M.R. 2013. Relationship between concrete resistivity and corrosion rate - A literature review, Cement and Concrete Composites, 39, 60-72.

[65] Cuzzilla, R., Di Ludovico, M., Prota, A., and Manfredi, G. 2011. Seismic rehabilitation of RC bridges by using FRP and SRP: case study of a bridge in the south of Italy, ACI-SP 277 (Recent Advances in Maintenance and Repair of Concrete Bridges), 1-20.

Table 1. Details of concrete mixture [1 MPa = 145 psi; 1 kg/m^3 = 0.062 lb/ft^3]

Component	Compressive strength (MPa)			
	30	35	40	45
wc	0.54	0.47	0.42	0.37
Water (kg/m³)	193	193	193	193
Cement (kg/m³)	358	406	455	524
Coarse aggregate (kg/m³)	1,144	1,144	1,144	1,144
Fine aggregate (kg/m³)	679	639	597	539

wc = water-to-cement ratio

Table 2. Modeling parameters [1 MPa = 145 psi; 1 mm = 0.0394 in.; 1 m = 3.28 ft]

Concrete strength, f'_c (MPa)	Construction method	Service environments	Concrete cover, c (mm)	Diffusion coefficient, $D(0)$ ($\times 10^{-12}$m^2/s)	Age parameter, η	Surface chloride, C_0 (% wt. of cement)	Corrosion initiation year, t_i (years)
30	CIP	Atmospheric	125	4.29	0.19	1.33	54.1
		Splash	125	6.43	0.019	$1.65t^{0.484}$	8.9
		Submerged	125	10.72	0.114	3.31	9.6
	ABC	Atmospheric	125	1.00	0.19	1.33	232.8
		Splash	125	2.30	0.019	$1.65t^{0.484}$	25.8
		Submerged	125	3.97	0.114	3.31	25.9
35	CIP	Atmospheric	100	3.15	0.295	1.17	55.6
		Splash	100	4.72	0.03	$1.37t^{0.484}$	8.8
		Submerged	100	7.87	0.177	2.93	9.1
	ABC	Atmospheric	100	0.73	0.295	1.17	238.9
		Splash	100	1.69	0.03	$1.37t^{0.484}$	25.5
		Submerged	100	2.91	0.177	2.93	24.5
40	CIP	Atmospheric	100	2.41	0.37	1.05	85.7
		Splash	100	3.62	0.037	$1.17t^{0.484}$	11.9
		Submerged	100	6.03	0.222	2.63	12.8
	ABC	Atmospheric	100	0.56	0.37	1.05	368.4
		Splash	100	1.29	0.037	$1.17t^{0.484}$	34.3
		Submerged	100	2.23	0.222	2.63	34.7
45	CIP	Atmospheric	85	1.75	0.445	0.92	108.3
		Splash	85	2.63	0.045	$0.97t^{0.484}$	12.7
		Submerged	85	4.38	0.267	2.29	14.2
	ABC	Atmospheric	85	0.41	0.445	0.92	465.7
		Splash	85	0.94	0.045	$0.97t^{0.484}$	36.7
		Submerged	85	1.62	0.267	2.29	38.3

CIP = cast-in-place; ABC = accelerated bridge construction

Table 3. Properties used for model validation [1 g = 0.0022 lb; 1 m = 3.28 ft]

Reference	Surface chloride	Diffusion coefficient (m^2/s)
Cao et al.[35]	0.5% wt. of concrete	3.22×10^{-12}
Titi and Biondini[36]	3% wt. of concrete	1×10^{-11}
Wang et al.[37]	$1.95\times(t/360)^{1.28715}$ mg/g*	$2.588\times(360/t)^{-0.9574}\times10^{-13}$
Yin and Pan[38]	2% wt. of binder	$1.38\times(28/t)^{-0.53}\times10^{-13}$

*: mass of chloride ions per mass of cementitious binder

t = time in days

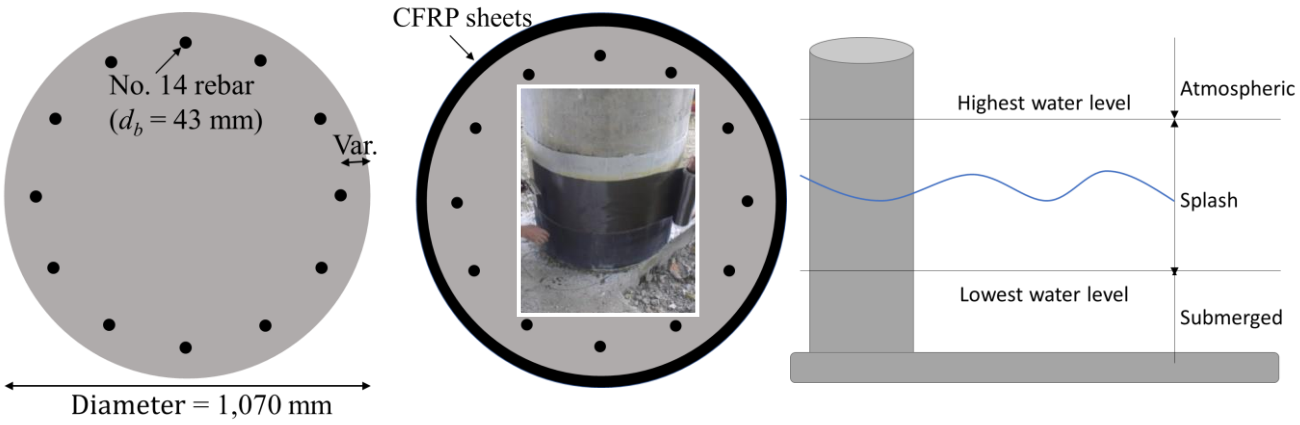

(a) (b)

[1 mm = 0.0394 in.]

Fig. 1. Benchmark column: (a) dimension and strengthening scheme (picture[65] used with permission, American Concrete Institute); (b) service environments

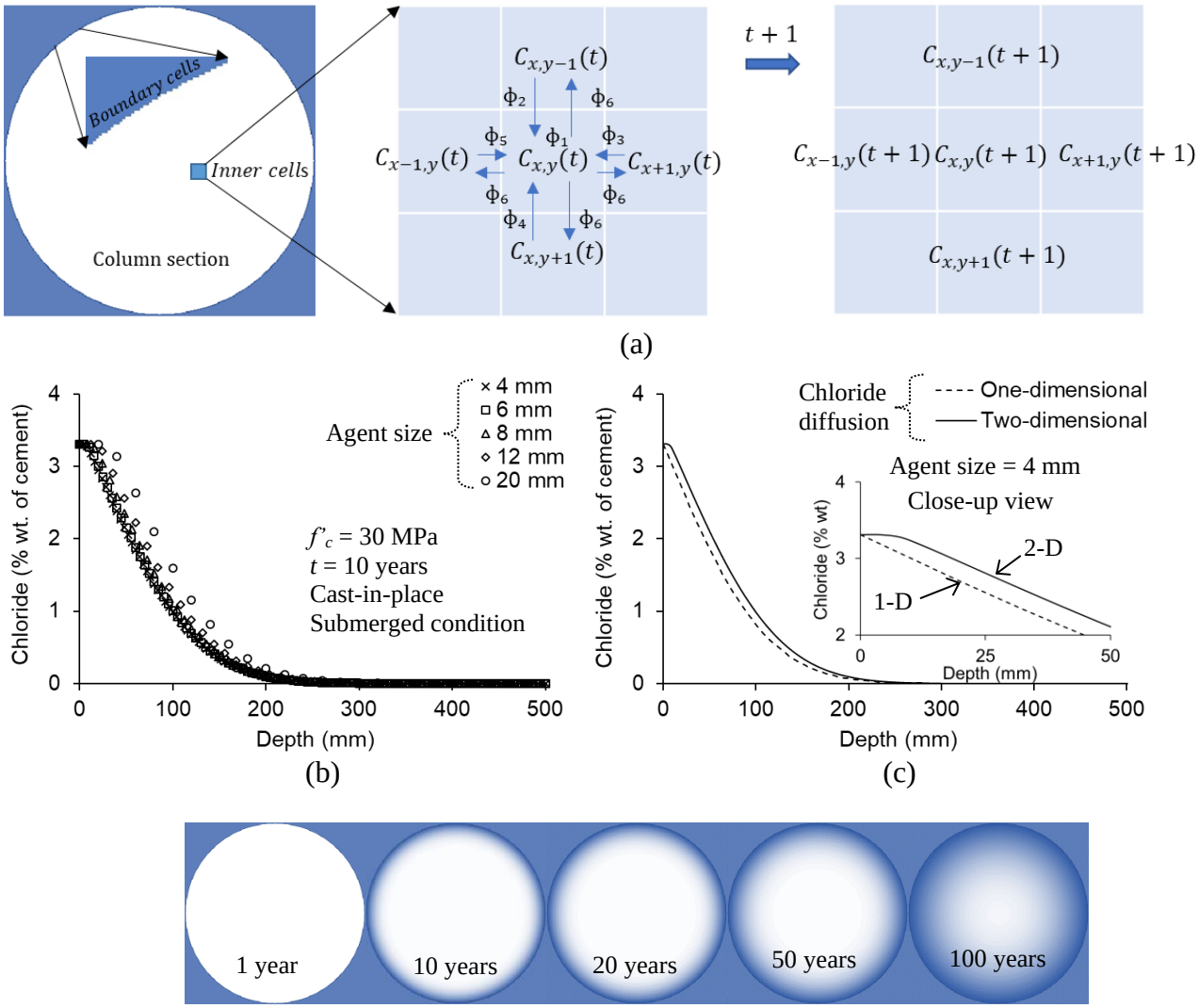

Fig. 2. Two-dimensional cellular automata for benchmark column: (a) configuration of von Neumann's square lattice; (b) sensitivity analysis; (c) proposed versus conventional approaches; (d) simulated chloride migration in cast-in-place column with concrete strength = 30 MPa under submerged condition

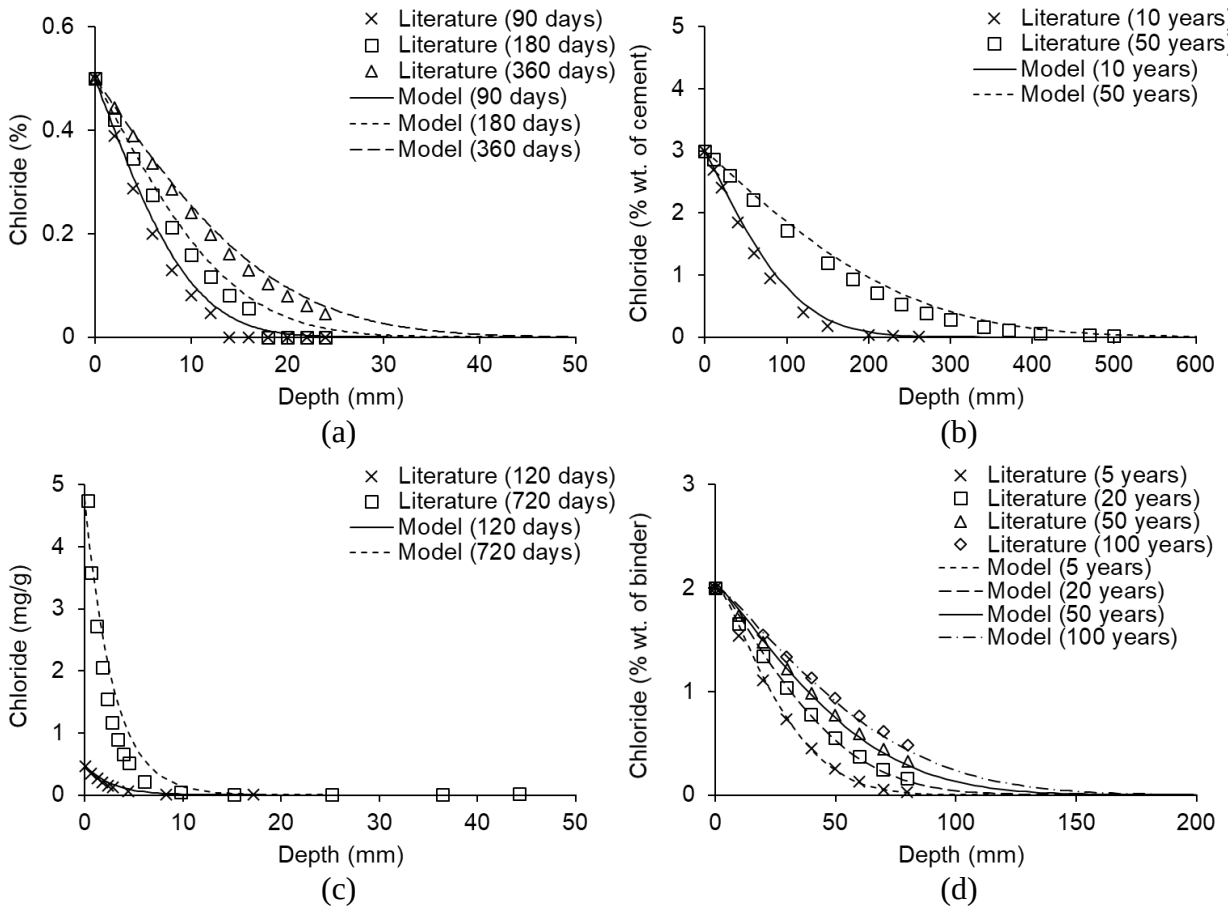

[1 mm = 0.0394 in.; 1 g = 0.0022 lb]

Fig. 3. Validation of modeling approach: (a) Cao et al.[35]; Titi and Biondini[36]; (c) Wang et al.[37]; (d) Yin and Pan[38]

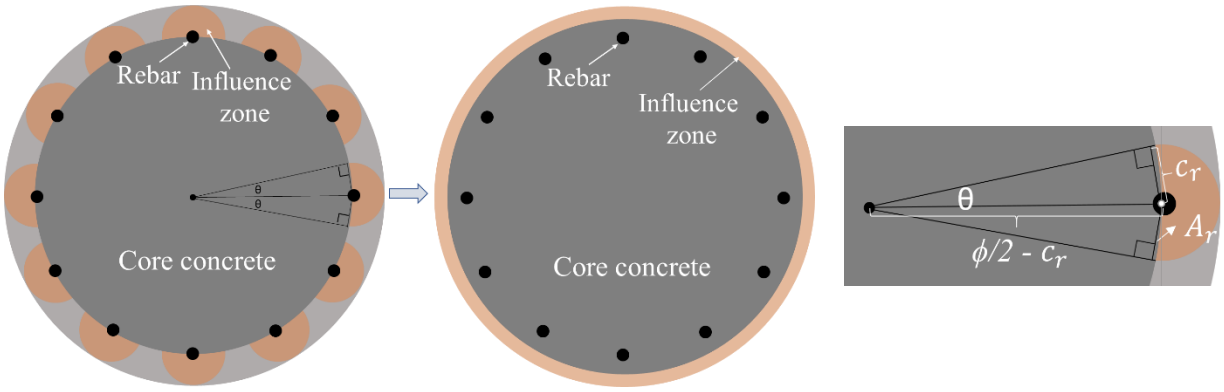

(a) (b) (c)

Fig. 4. Cover-strength reduction: (a) spalling and cracking zones; (b) equivalent area; (c) geometric details

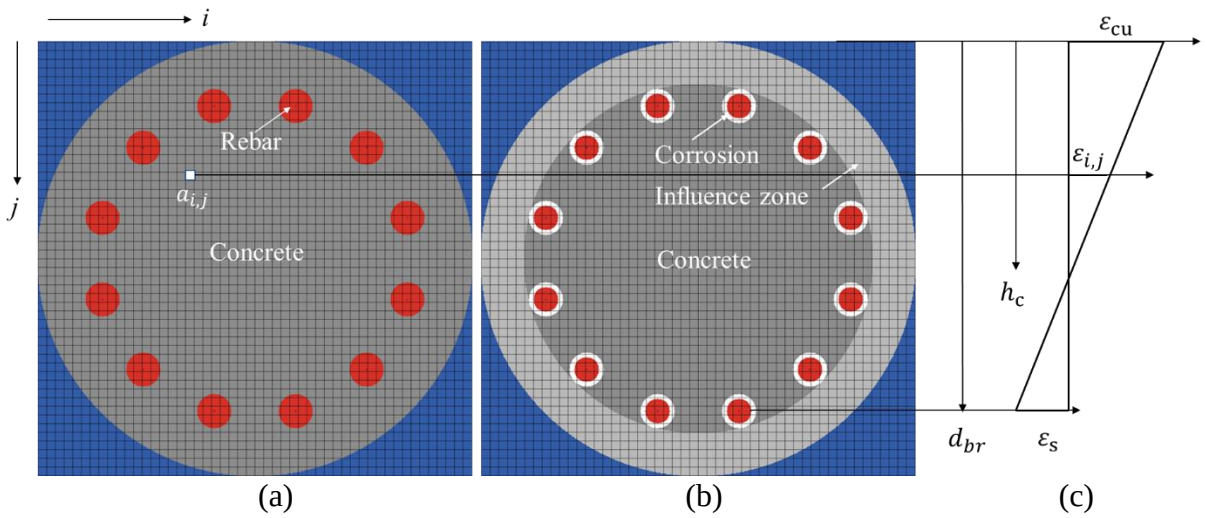

Fig. 5. Sectional model: (a) intact column; (b) corrosion-damaged column; (c) strain profile

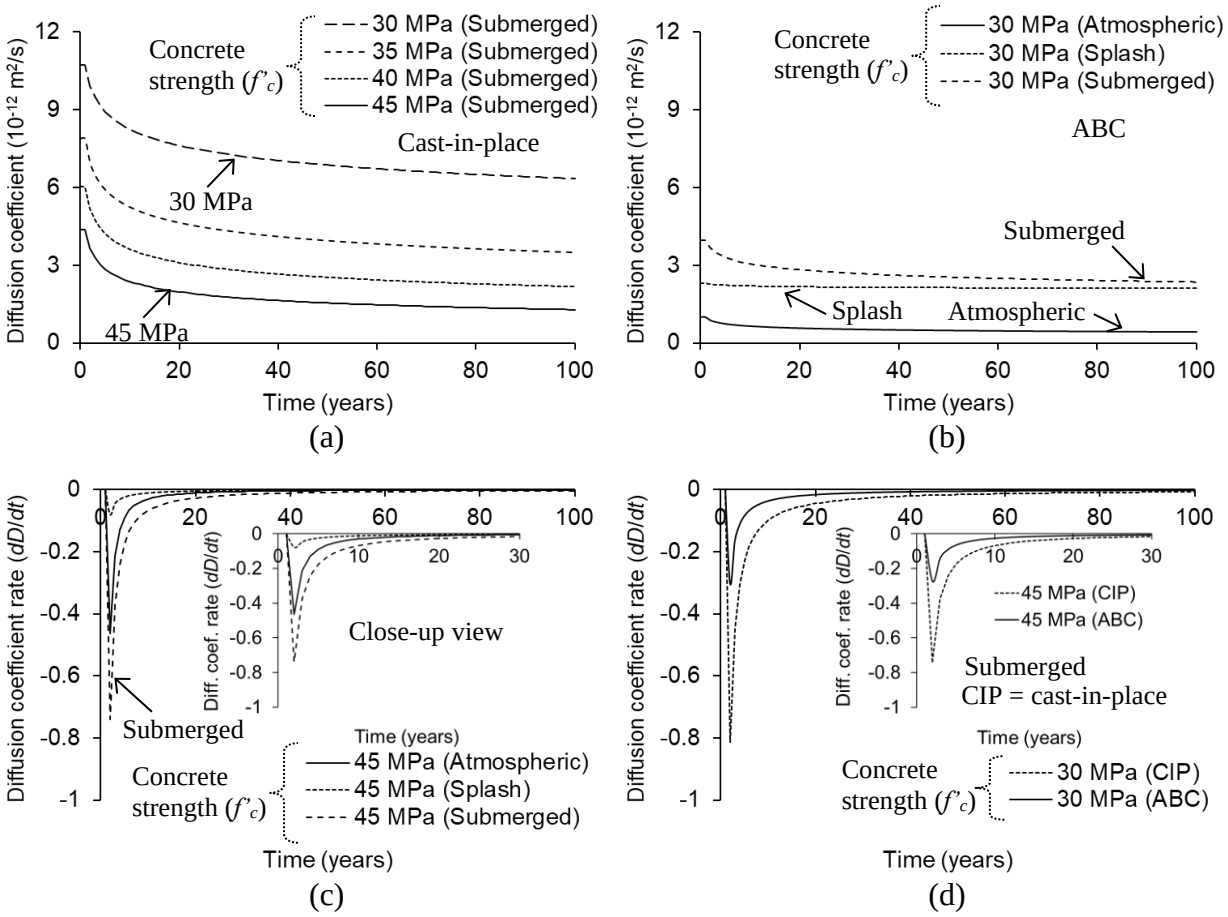

[1 m = 3.28 ft; 1 MPa = 145 psi]

Fig. 6. Diffusion coefficient: (a) cast-in-place column with concrete strength; (b) ABC column with service environment; (c) rate in cast-in-place column with service environment; (d) comparison of rates between cast-in-place and ABC columns under submerged condition

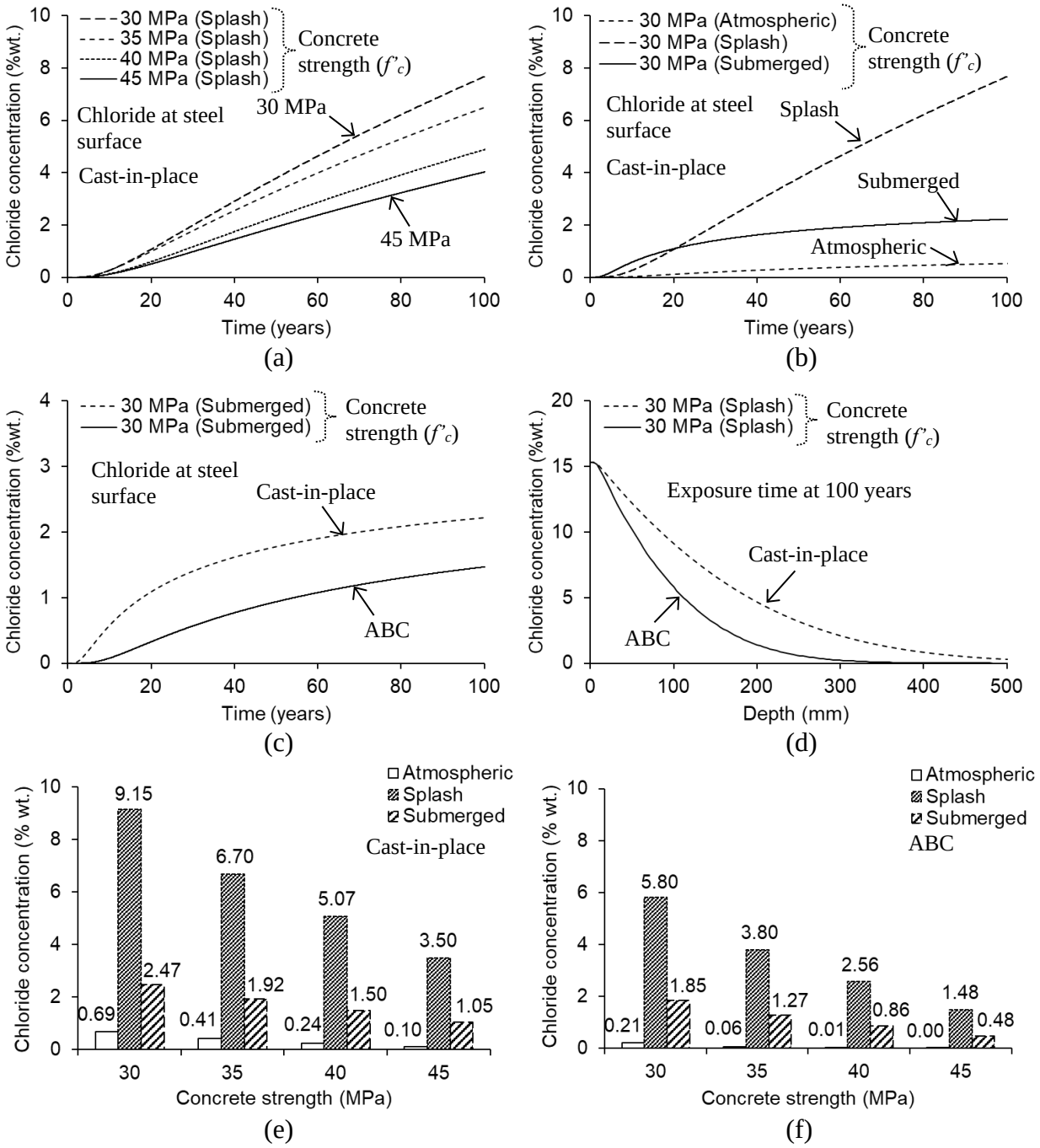

[1 mm = 0.0394 in.; 1 MPa = 145 psi]

Fig. 7. Chloride concentration: (a) cast-in-place column with concrete strength; (b) cast-in-place column under variable environments; (c) cast-in-place vs. ABC columns with time; (d) cast-in-place vs. ABC columns across concrete; (e) cast-in-place column at 100 mm from surface; (f) ABC column at 100 mm from surface

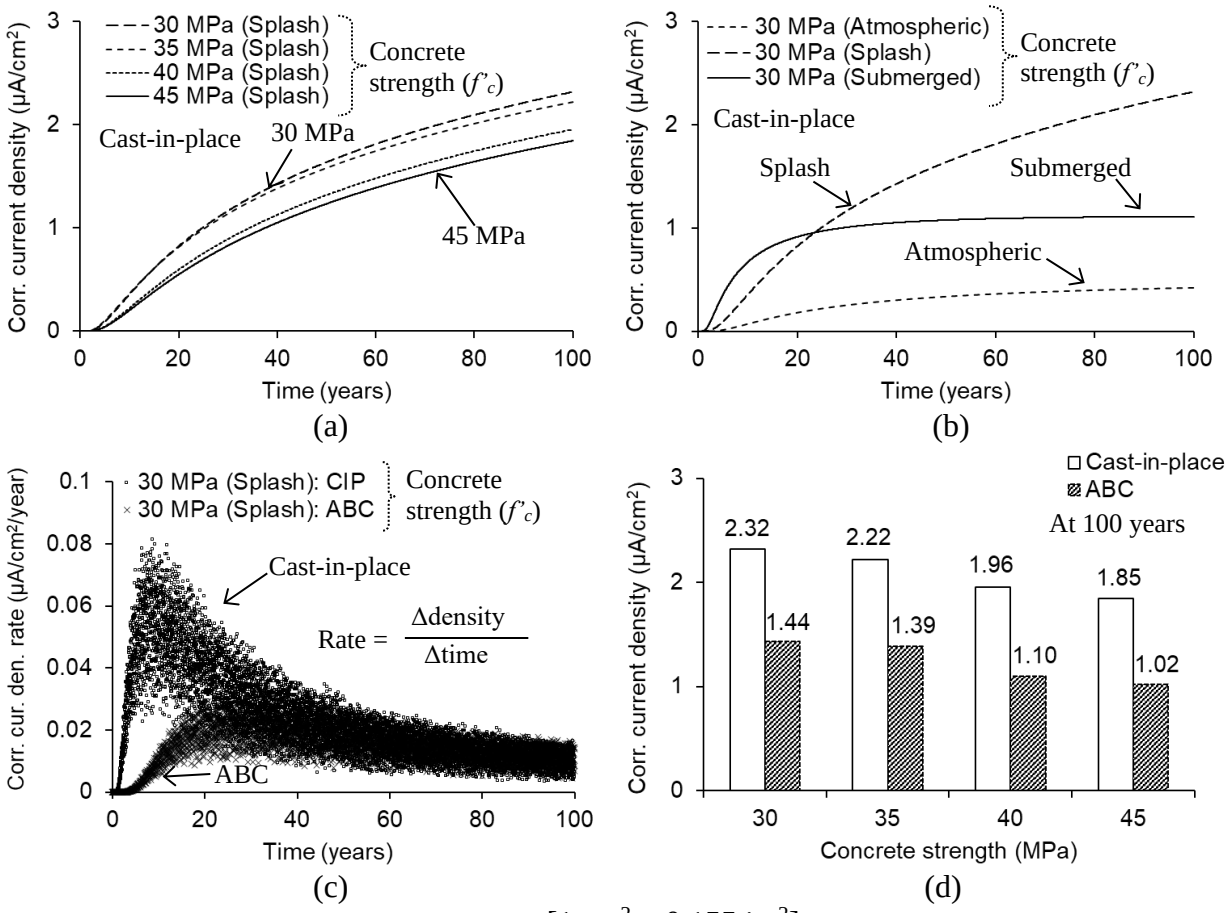

Fig. 8. Corrosion current density at surface level of reinforcement: (a) cast-in-place column with concrete strength; (b) cast-in-place column under variable environments; (c) cast-in-place vs. ABC columns with time; (d) comparison at 100 years

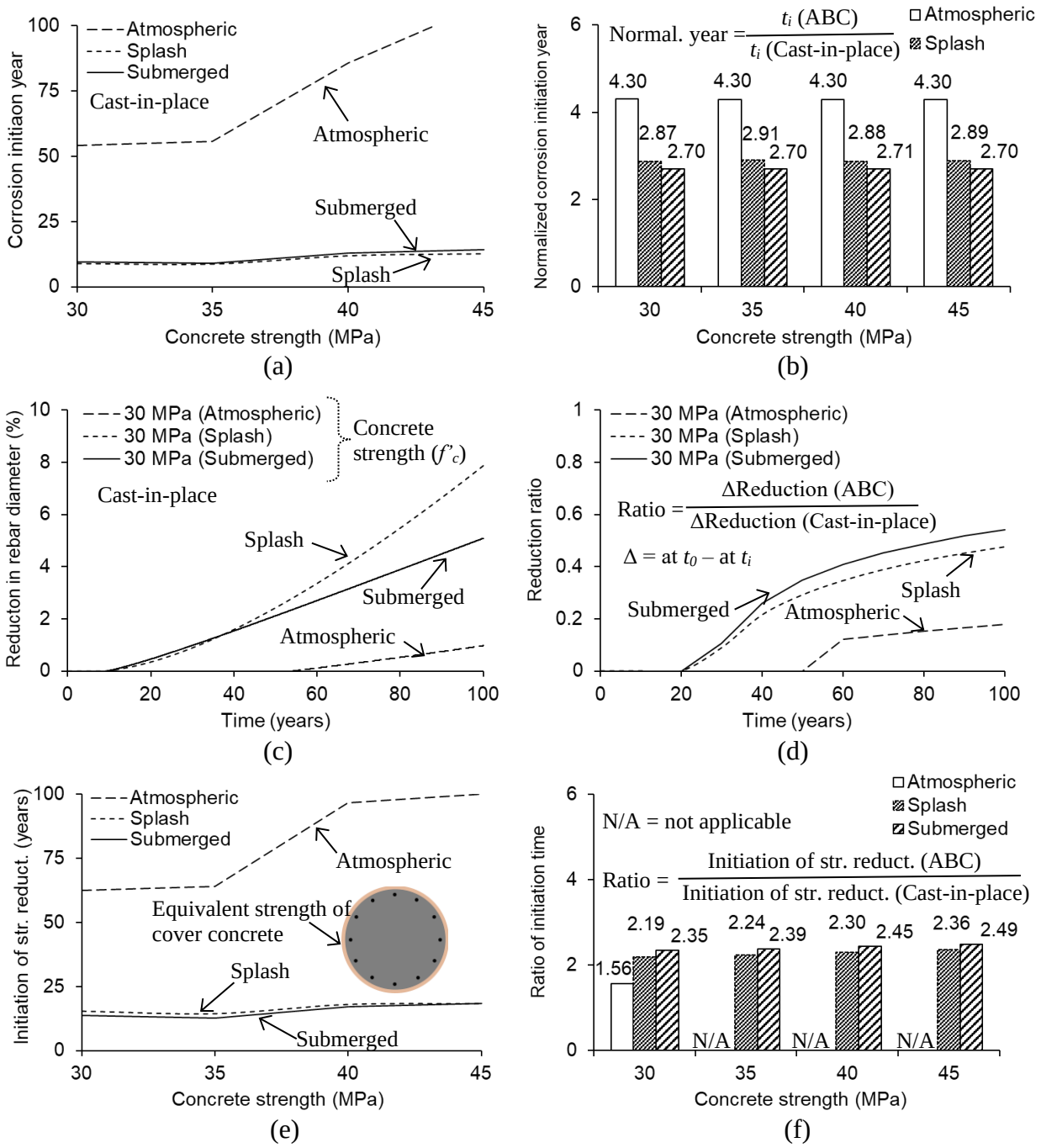

Fig. 9. Consequences of corrosion: (a) corrosion initiation year for cast-in-place column; (b) normalized corrosion initiation year; (c) reduced rebar diameter in cast-in-place column; (d) ratio of reduced rebar diameter between ABC and cast-in-place columns; (e) initiation of strength reduction in cover concrete of cast-in-place column; (f) ratio of initiation time for strength reduction between ABC and cast-in-place columns

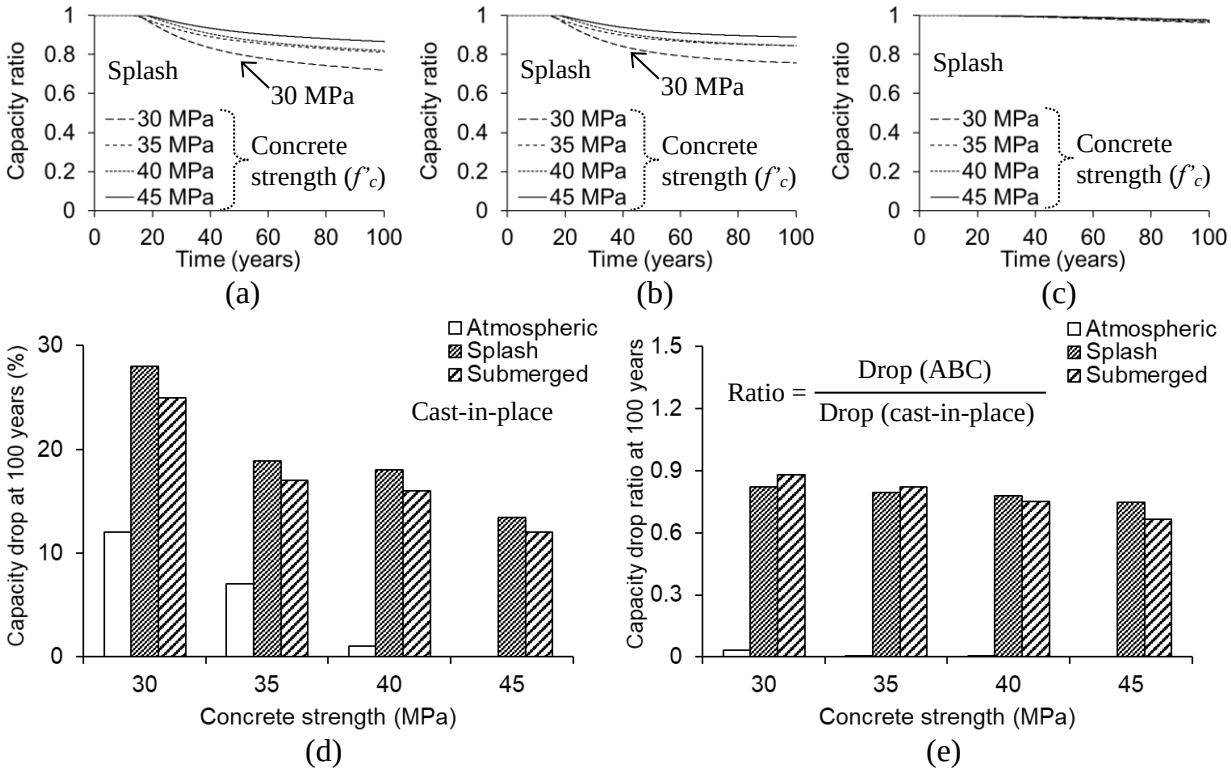

Fig. 10. Reduction in axial capacity of column: (a) normalized capacity of cast-in-place column; (b) concrete portion of normalized capacity; (c) rebar portion of normalized capacity; (d) capacity drop of cast-in-place column at 100 years; (e) ratio of capacity drop between ABC and cast-in-place columns at 100 tears

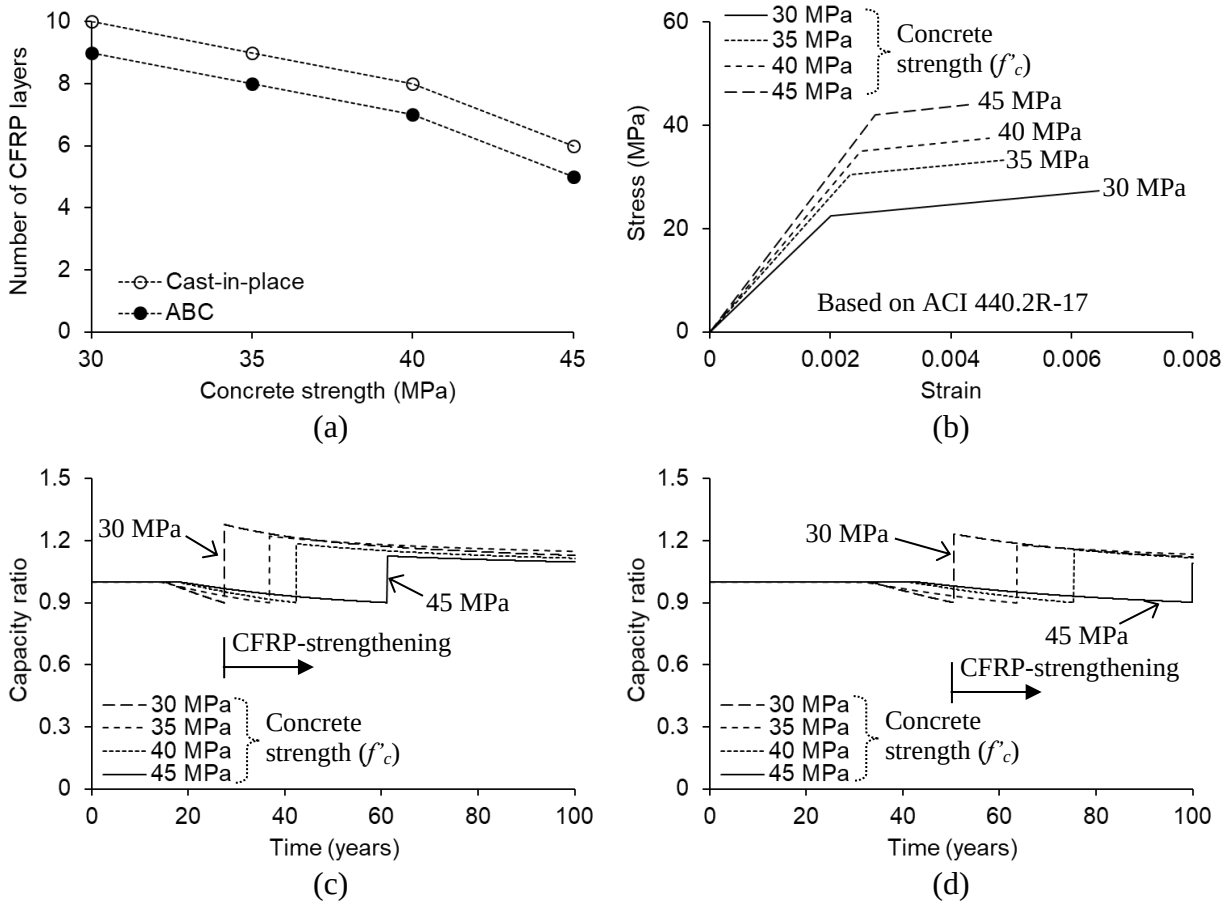

Fig. 11. Strength recovery with CFRP-confinement: (a); CFRP layers (b) stress-strain relationship of cast-in-place concrete (f'_{cc}); (c) cast-in-place column; (d) ABC column

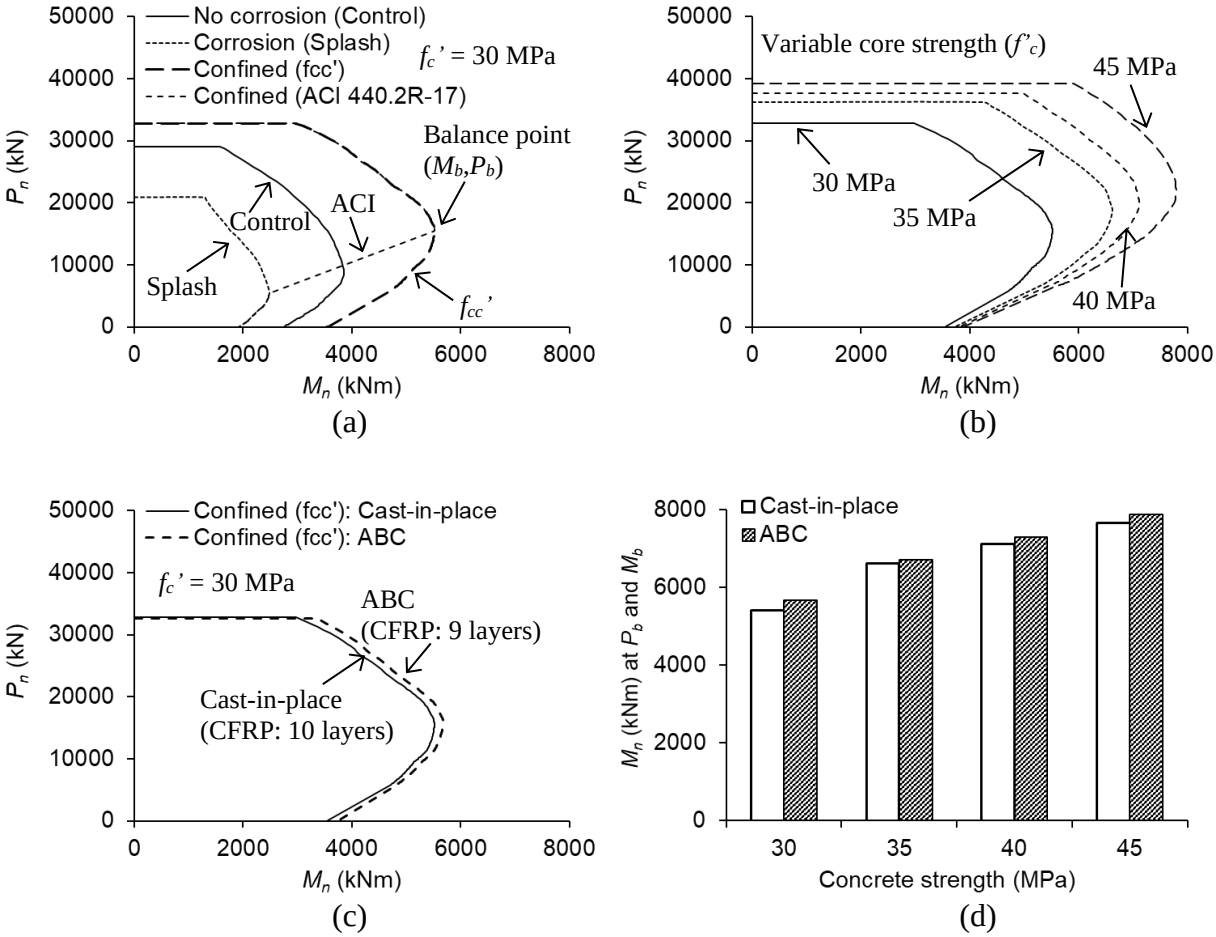

Fig. 12. Load-moment interaction at 100 years: (a) cast-in-place column; (b) cast-in-place column confined with f'_{cc}; (c) cast-in-place vs. ABC columns; (d) comparison at balance load (P_b) and moment (M_b)